

Electrochemical Synthesis of Nickel Oxide Nanoparticulate Films on Nickel Foils for High-performance Electrode Materials of Supercapacitors

Hong-Ying Wu* and Huan-Wen Wang

College of Chemistry and Chemical Engineering, Northwest Normal University, Lanzhou 730070, PR China

*E-mail: hongying8860@163.com

Received: 13 March 2012 / Accepted: 6 April 2012 / Published: 1 May 2012

The ultrahigh pseudocapacitive nickel oxide nanoparticulate films on the nickel foils are prepared through a two-step in which nickel hydroxides are electrodeposited on the nickel substrate in 0.08 M Ni(NO₃)₂ aqueous solution and then they are thermally transformed into uniform nickel oxide nanoparticles. The morphology, structure and electrochemical property of the samples are characterized in detail. The high specific capacitance of 1478 F g⁻¹ with excellent rate capability and long cycle ability is obtained in the case of nickel oxide nanoparticulate film calcined at 250 °C. The loose structure composed of the interconnected nanoparticles as well as the intimate contact between nickel oxide and nickel substrate is responsible for the outstanding capacitive performance of resulting materials. In addition, the especial properties of the electrodeposited nickel hydroxide, such as high water content and lower conversion temperature, are discussed in detail.

Keywords: Nickel oxide, Nanoparticulate film, Electrodeposition, High-performance, Supercapacitors

1. INTRODUCTION

Supercapacitors are charge storage devices which have a greater power density and longer cycle life than batteries, and a higher energy density than conventional capacitors [1]. To improve the performance of supercapacitors, many compounds are investigated as the electrode materials, including carbonaceous materials [2, 3], conducting polymers [4, 5] and transition-metal oxides/hydroxides [6-12]. The last two materials involve with pseudo Faradic reactions, unlike carbon materials, which generate the double-layer capacitance because of the separation of charge at the interface between the solid electrode and an electrolyte [13]. In recent years, transition metal oxides have drawn extensive and intensive research attention due to their potentially high specific

capacitance. Among them, RuO₂ is considered as the most prominent material offering high specific capacitance (1580 F g⁻¹) with excellent cyclability to replace carbonaceous materials which are commercialized [14]. However, the practical applications may be embarrassed by the high cost and rareness of ruthenium. Consequently, alternative materials with less cost are being searched for.

Nickel oxides are potential for applications of electrode materials in supercapacitors due to their high electrochemical reaction activity [15]. A loose-packed flake-like NiO synthesized by using a chemical precipitation method had been proved to exhibit a specific capacitance of 942 F g⁻¹ [16]. The mesoporous NiO [17] and NiO/MWCNTs composite [18] were also used as electrode materials of supercapacitors, and achieved specific capacitance of 165 F g⁻¹ and 384 F g⁻¹ respectively. Recently, the nickel oxide film with nanoflakes and open macropores was prepared by electrophoresis and electrodeposition, and showed a specific capacitance of 351 F g⁻¹ [19]. However, the specific capacitance of these nickel oxides as electrode materials is still far from their theoretical value (3228 F g⁻¹ within 0.4 V), indicating the low utilization of the nickel oxide matrix. Therefore, it is necessary to optimize the macrostructures of NiO through appropriate strategies to enhance both the energy density and power density.

It is known to all that nano-structures lead to a high utilization of materials [20]. Particularly, nano-structured electrode materials show better performances than traditional materials [21] because of the distance within the material over which electrolyte ions transport is shorter. With respect to fabrication of nanostructured electrode materials, the important issue is focused on not only controlling the size and the geometry but also considering the simplicity and low cost of the synthesis methods. Compared with the normal synthesis techniques, such as the sol-gel process [22], hydrothermal process [23] and chemical precipitation [24], the advantages of using the electrochemical strategy are simplicity, reliability, accuracy, versatility, and low cost.

In the present work, we report a simple electrochemical strategy to prepare loosely packed nickel oxide nanoparticulate films for electrode materials of supercapacitors, in which the nickel hydroxide electrodeposited on nickel substrate in 0.08 M Ni(NO₃)₂ aqueous solution is transformed into the nickel oxide films through a subsequent thermal treatment. Interestingly, the nickel hydroxide prepared by electrochemical depositions is more unstable or easier to be converted into the nickel oxide at lower temperature because of its high water content and large inter-sheet distance. We used this advantage to synthesize nickel oxide nanoparticulate films with loose structure, which is beneficial to enhancing the pseudocapacitive properties of electrode materials. Electrochemical measurements show that the nickel oxide film calcined at 250 °C reaches an ultrahigh specific capacitance of 1478 F g⁻¹ (the highest ever reported for nickel oxides) in 1 M KOH aqueous solution electrolyte, implying that the resulting nickel oxide nanoparticles on the nickel foils are promising candidates for supercapacitor electrode materials.

2. EXPERIMENTAL

2.1 Synthesis of films

Reagents are all of AR grade. Water used in the synthesis and washing is deionized. Research

grade nickel foil was purchased from Shanghai metal foil plant. The nickel foil was polished with emery paper to a rough finish, washed in an ultrasonic bath of acetone, dilute NaOH solution, dilute HNO₃ solution and deionized water in turn for 10 min, and then air-dried prior to usage. The nickel hydroxide was deposited on the nickel foil in 0.08 M Ni(NO₃)₂ aqueous solution at a potential of -0.90 V vs. SCE electrode to give a totally passed charge of 0.5 C for the same required amount of nickel oxide which was estimated by Faraday's law. The electrodeposition was carried out using a Chenhua CHI660B model Electrochemical Workstation (Shanghai) with a three-electrode cell which consists of nickel foil working electrode (1 cm² in area), a platinum foil counter electrode and a standard calomel electrode (SCE) reference electrode. After the deposited nickel hydroxide electrode was washed with deionized water several times, and then left to dry at room temperature, the nickel oxide nanoparticulate films were formed through thermal treatment in air at desired temperatures for 2 h with a rate of 5 °C min⁻¹ in muffle stove.

2.2 Characterization

The samples scraped from nickel foil were examined by X-ray diffraction (XRD) (D/Max-2400) with Cu K α radiation ($\lambda = 1.5418 \text{ \AA}$) operating at 40 kV, 100 mA. The morphology was observed by field emission scanning electron microscopy (FESEM) (JSM-6701F, Japan). Thermal analyses, including thermogravimetry and differential thermogravimetry (TG-DTG), were carried out using a Perkin-Elmer TG/DTA-6300 instrument in the temperature range of 25–750 °C. A heating rate of 10 °C min⁻¹ in nitrogen with a flow rate of 20 mL min⁻¹ was used.

Electrochemical characterization was carried out in a three-electrode electrochemical cell which contains 1 M KOH aqueous solution as electrolyte. The as-prepared nickel oxide films on nickel foils were directly used as the working electrode, a platinum foil as counter electrode, and SCE as reference electrode. Cyclic voltammetry (CV), galvanostatic charge-discharge and electrochemical impedance spectroscopy (EIS) were performed on a CHI660B electrochemical working station at room temperature.

3. RESULTS AND DISCUSSION

3.1. Material characterization

The TG and DTG curves of the deposited nickel hydroxide were shown in Fig. 1. Fig. 1 displays the weight loss of the nickel hydroxide in two steps. The first step corresponds to the first peak on the DTG curve and arises due to the presence of the adsorbed and intercalated water molecules. The dehydration starts at 60 °C and proceeds until completion up to 200 °C, which is accompanied by a 16% loss in mass. This weight loss is much greater in comparison with dehydration of the nickel hydroxide synthesized by chemical precipitation [25], implying that the nickel hydroxide prepared by electrodeposition contains more intercalated water molecules. The second step corresponds to the second peak on the DTG curve and results from the decomposition of nickel

hydroxide. Most of the weight loss occurs at 250 °C, but an extended flanking loss is seen up to 400 °C. This result is caused by dehydroxylation of the hydroxide layers combined with the loss of the anionic species (NO_3^- and CO_3^{2-}). TG analysis shows that the total weight loss for the electrodeposited nickel hydroxide is up to 40%, as noted by other authors [26].

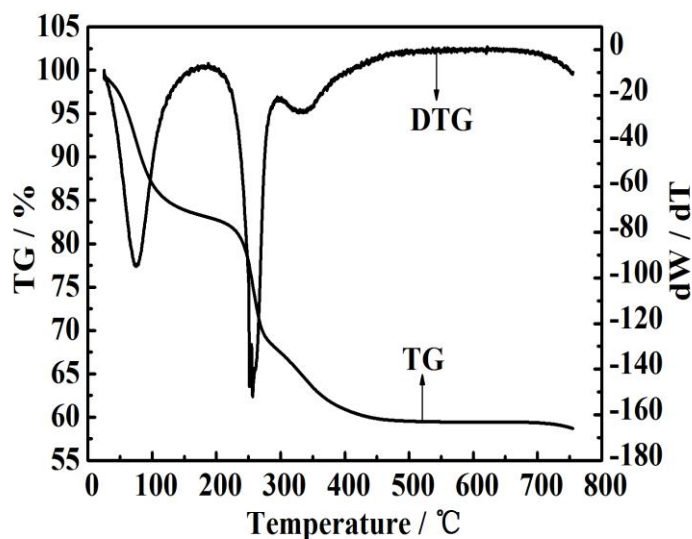


Figure 1. TG/DTG curves of the nickel hydroxide film.

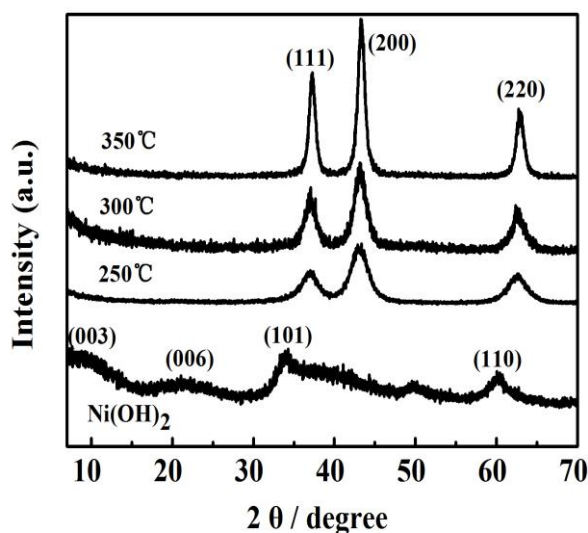


Figure 2. XRD patterns of the nickel hydroxide film and the nickel oxide films calcined at different temperatures.

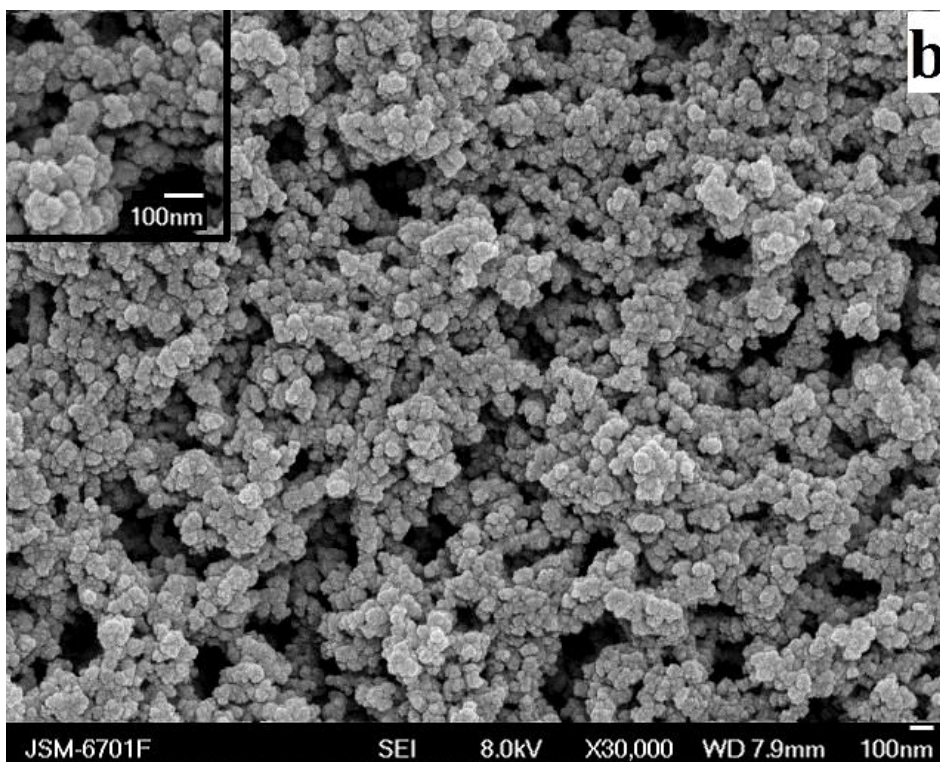
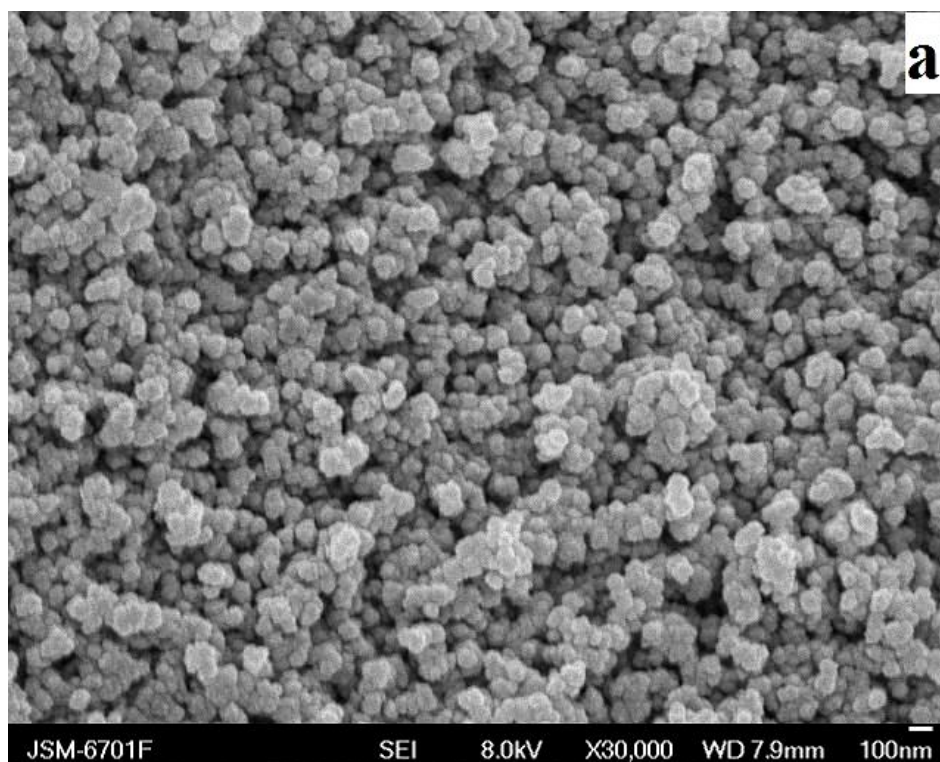
The crystal phase and structure information of the products were obtained by XRD measurements. Fig. 2 shows XRD patterns of the $\text{Ni}(\text{OH})_2$ prepared by electrodeposition and the nickel oxides produced by thermally treating the electrodeposited $\text{Ni}(\text{OH})_2$ at different temperatures. XRD

pattern of the $\text{Ni}(\text{OH})_2$ shows peaks at $d = 10.2, 3.81, 2.63,$ and 1.54 \AA , which could be assigned to (003), (006), (101) and (110) planes. All the peaks indicate the formation of α -type nickel hydroxides (JCPDS, No. 38–0715). The third diffraction peak has the typical broad “saw-tooth” shape, with a sharp rise at the low-angle side and pronounced asymmetry on the high-angle side, indicating that layer stacking in the hydroxide must be rather loose and defective. In the hydrotalcite-like compounds, the lattice parameter “a” corresponds to the average cation-cation bond distance within a given layer, while parameter “c” corresponds to several times the thickness of an elemental “sandwich”. The first parameter depends mostly on the ionic radii of the layer cations, while the second one depends on the size of the intercalated anion and on its orientation in the interlayer (in the case of nonspherical anions), as well as on the electrostatic interaction between the interlayer species and the layers. XRD data shows that the inter-sheet distance (c spacing) of the electrodeposited nickel hydroxide is up to 10.2 \AA , which is much larger than the normal inter-sheet distance (7.6 \AA) of the α -type nickel hydroxide. The big expansion in interlayer spacing makes the stacking of the layers more disordered and the sample more unstable thermodynamically, so a lower temperature in converting nickel hydroxide to nickel oxide is observed. As seen from Fig. 2, all of the hydroxide is converted into NiO (JCPDS, No. 22–1189) after the thermal treatments above $250 \text{ }^\circ\text{C}$. This is also in agreement with the TG–DTG analysis presented in Fig 1, which shows a sharp drop in the weight at around $250 \text{ }^\circ\text{C}$ accompanied by the conversion reaction. The grain size of nickel oxides at $250, 300$ and $350 \text{ }^\circ\text{C}$, which was estimated from the major diffraction peak (200) by using the Debye-Scherrer equation, is $3.48, 5.28$ and 9.71 nm , respectively.

It should be pointed out that the high water content and large inter-sheet distance in the nickel hydroxide prepared by electrodeposition are associated with electrochemical reaction conditions. When electric current passes on, the nitrate ions in the electrolyte are reduced on the cathodic surface to produce hydroxide ions, resulting in the deposition of nickel hydroxide on the electrode surface. The extra nickel ions move from bulk solutions to cathodic surface under the influence of an electric field, which makes the positive ions over sufficient in the vicinity of the cathodic surface. Hence, the stacking $\text{Ni}(\text{OH})_{2-x}$ layers contain more hydroxyl vacancies, which leads an increasing of c spacing and defects because of the higher electrostatic repulsion within the layers. In order to satisfy the principle of charge neutrality and minimum energy, numerous water molecules and nitrates would be intercalated in the interlayer space, which was confirmed by the FT-IR spectrum of the electrodeposited nickel hydroxide presented in our previous work [27]. It is believed that the electrodeposited nickel hydroxide is unstable due to the disorders and larger intersheet distance, and so its decomposition takes place at lower temperatures, as shown in Fig. 2. In the transformation from the hydroxide into the oxide, the temperature is an important factor to obtain fine particles. The less grain size of nickel oxide is formed easily at a lower temperature. Therefore, the electrodeposition is advantageous for preparing the electrode materials of nickel oxide.

The surface morphologies of the nanoparticulate films were imaged by FESEM in Fig. 3. It can be seen from Fig. 3(a) that the $\text{Ni}(\text{OH})_2$ film consists of uniform and pretty dense particles with sizes in the range of 90 nm . The FESEM image of the nickel oxide film calcined at $250 \text{ }^\circ\text{C}$ is showed in Fig. 3(b). A loosely packed network assembled by spherical particles with diameter in the range from 30 to

50 nm is obviously observed. The further observations (as shown in the upper left inset) indicate that the big particles are composed of several small nanoparticles.



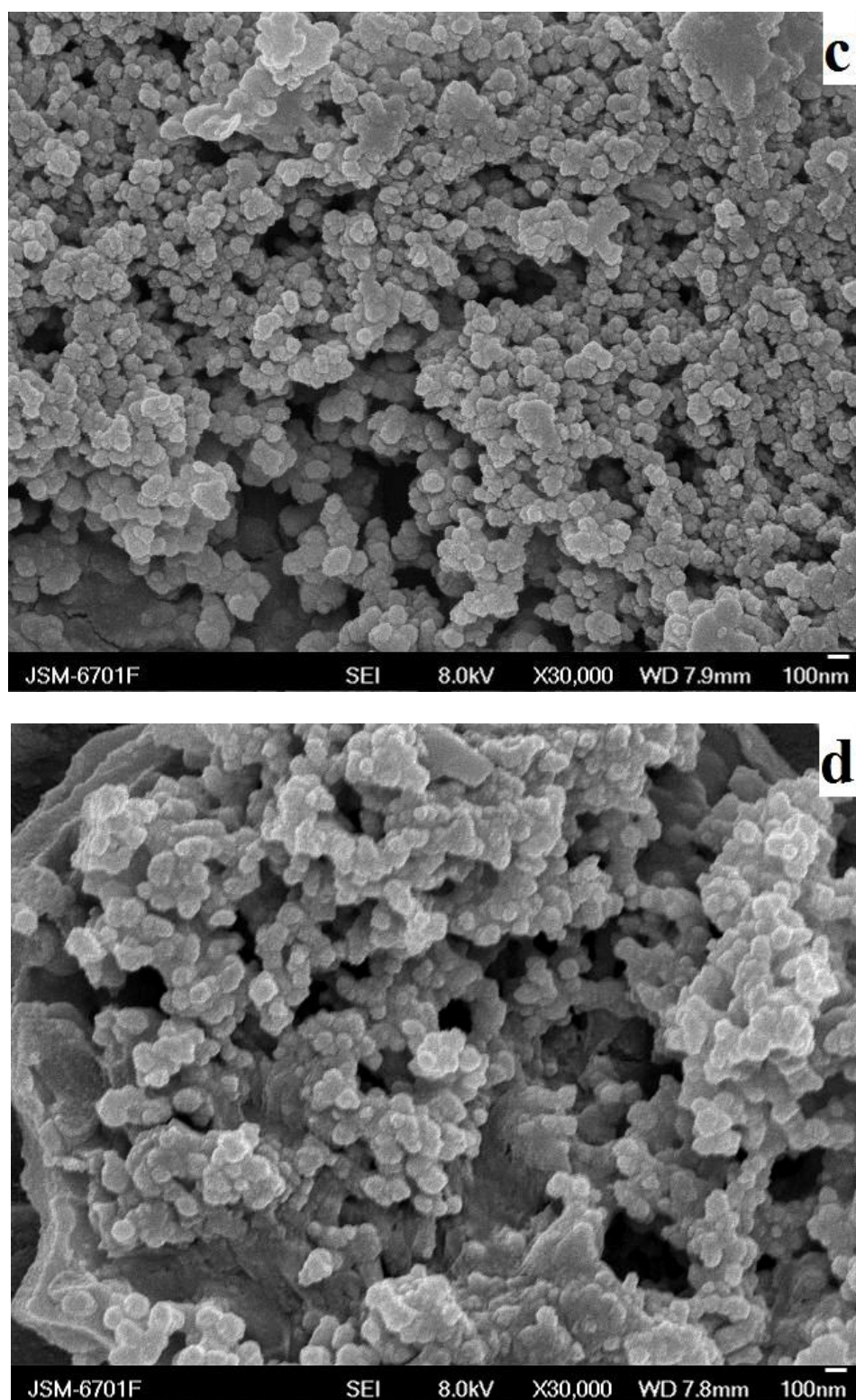


Figure 3. FESEM images of the nanoparticulate films: (a) the nickel hydroxide film obtained at -0.90V vs. SCE and the nickel oxide films calcined at (b) 250, (c) 300, and (d) 350 °C, respectively.

It is worth noting that the small nanoparticles observed in Fig. 3(b) might contain a number of particles with the grain size of 3.48 nm (XRD analysis in Fig. 2), implying that the loose structure

exists in the exterior and interior nickel oxide particles. This unique structure or morphology makes electrolyte ions not only penetrated into the outer region of the film but also the inner region, which is able to increase the liquid–solid interfacial area, provide a path for the insertion and extraction of ions, and ensure a high reaction rate. Fig. 3(c) shows the morphology of the nickel oxide film calcined at 300 °C. Obviously, the agglomeration of particles occurs. Furthermore, the aggregations become serious with increasing calcination temperature, as shown in Fig. 3(d).

3.2. Electrochemical characterization

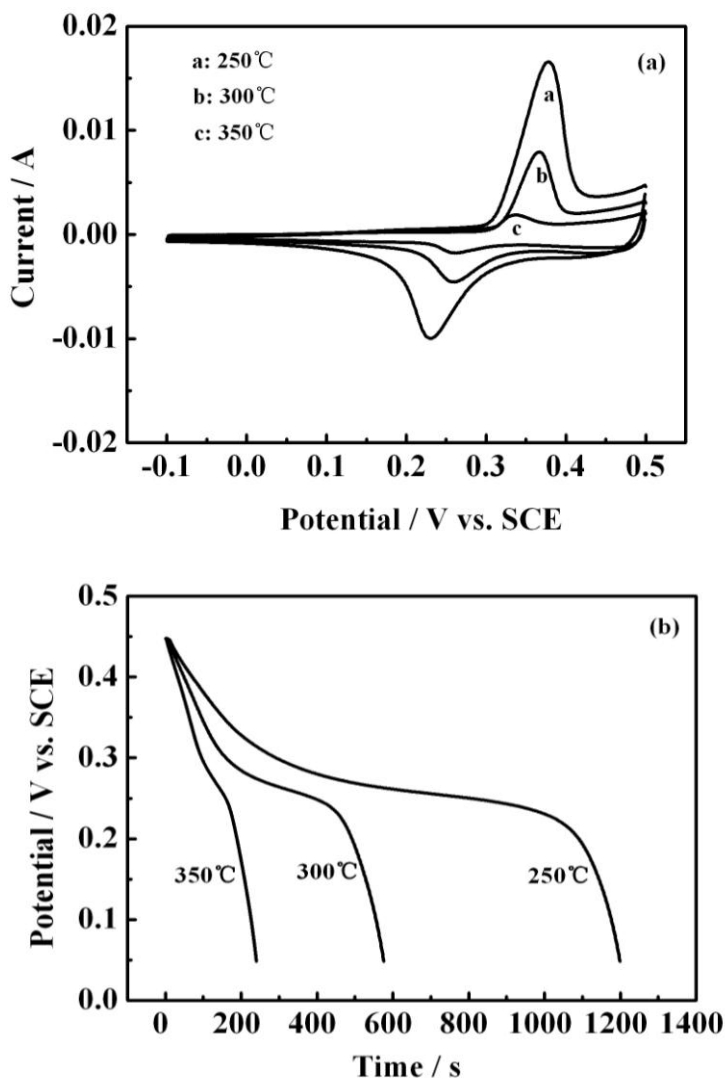


Figure 4. Electrochemical properties of the nanoparticulate nickel oxide films calcined at different temperatures in 1 M KOH solution: (a) CV curves within a potential window of -0.1 to 0.5 V vs. SCE and (b) discharging curves in the potential range from 0.05 to 0.45 V at a current density of 0.5 A g^{-1} .

In order to investigate the influence of thermal treatment temperature on the capacitance of the films, CVs of the different samples were performed in the potential window from -0.1 to 0.5 V. Fig.

4(a) shows the CV curves of the nanoparticulate nickel oxide film electrodes calcined at 250 °C, 300 °C, and 350 °C in the 1 M KOH solution. As shown in the curves, there is a pair of strong redox peaks due to a result of the Faradaic reactions of the NiO. It is well known that the faradic reaction of the NiO electrode materials will proceed according to the following reaction [28]:



One quasi-reversible electron transfer process is visible in every curve, indicating that the measured capacitance is mainly based on redox mechanism [29]. Besides, the integral area of the CV loops is maximal for the sample calcined at 250 °C, but minimal for the sample at 350 °C.

Fig. 4(b) shows discharge curves of the samples obtained at different calcination temperature in 1 M KOH electrolyte under 0.5 A g⁻¹ in the potential range of 0.05 to 0.45 V. The specific capacitance is calculated by $I \times t / (V \times m)$, where I is the discharging current, t is the discharging time, V is the potential drop during discharge, and m is the mass of the nickel oxide [30]. The specific capacitance values calculated from the discharging curves are 1478, 710 and 296 F g⁻¹ for the nanoparticulate films calcined at 250, 300 and 350 °C, respectively. Obviously, the nickel oxide film obtained at 250 °C exhibits the maximum specific capacitance, which is in agreement with the result of the CV test. The sharp decline of the specific capacitance with increasing the calcination temperature is observed clearly. This can be explained: (i) For the nickel oxide electrode calcined at 250 °C, the unique nanoparticulate film with loosely packed network not only facilitates the penetration of electrolytes into the whole oxide matrix, but also increases the liquid–solid interfacial area. (ii) Once the oxide phase is formed, further heat treatment at higher temperature may cause the increase in grain size, and accordingly a decrease both in specific surface area and reactivity for surface chemical processes, thereby leading to a low capacitance [16, 31]. This can be also illustrated from surface morphologies and XRD patterns of nickel oxides presented in Fig (2, 3), which shows a large increase in agglomeration and grain size at increasing calcination temperature. (iii) Just like RuO₂, the specific capacitances may also depend on hydration and crystallinity of nickel oxide [32].

Further electrochemical investigation is focused on the nanoparticulate nickel oxide film electrode calcined at 250 °C. As seen from Fig. 5(a), the characteristic CV shapes of the nickel oxide film are not significantly influenced with the increasing of the scan rates. This indicates an excellent capacitance behavior, low equivalent series resistance (ESR) and the fast diffusion of electrolyte ions into the film. In order to display cyclic voltammetric characteristic of the electrode, the response of the anodic current to sweep rates was measured. It can be seen from the inset of Fig. 5(a) that the anodic peak current i_p vs. V plot, where V is the voltage scan rate, gives a reasonable linear relationship. In comparison with metal hydroxides [12, 27], where i_p vs. $V^{1/2}$ gives a linear relationship regardless of scan rate for a kinetically uncomplicated redox reaction, this result indicates that the charge-storage mechanism of the nanoparticulate nickel oxide film is not a diffusion-controlled reaction but a fast redox reaction at the electrode/electrolyte interface. This is a typical behavior of the ideal supercapacitor materials.

Fig. 5(b) displays the discharge curves of the nanoparticulate nickel oxide film electrode calcined at 250 °C at different current densities. The specific capacitance values are calculated to be

1478, 1365, 1214, and 1086 $F g^{-1}$ corresponding to current densities of 0.5, 1, 4, and 8 $A g^{-1}$, respectively. The relatively small decrease in capacitance is caused by the increment of voltage (IR) drop. It means that sufficient active material is involved in the redox reaction under higher current densities [30]. This result implies that the nickel oxide film electrode has a good rate capability at a large current density, which is very important for the electrode materials of a supercapacitor to provide high power density.

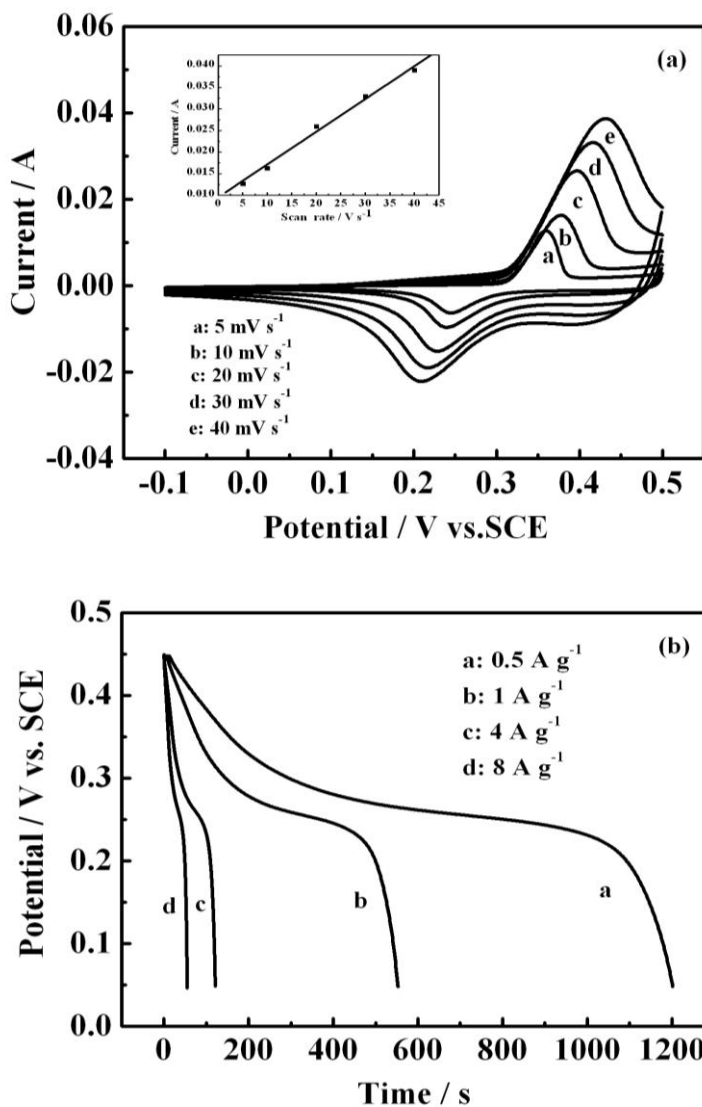


Figure 5. Electrochemical properties of the nanoparticulate nickel oxide film electrode calcined at 250 $^{\circ}C$ in 1 M KOH solution: (a) CV curves at different scan rates within a potential window of -0.1 to 0.5 V vs. SCE. The inset shows variation of anodic peak current with scan rate. (b) discharge curves in the potential range from 0.05 to 0.45V at different current densities.

The EIS analysis has been recognized as one of the principal methods for examining the fundamental behavior of electrode material for supercapacitors. The EIS spectra of the nanoparticulate nickel oxide film electrode calcined at 250 $^{\circ}C$ are shown in Fig. 6. The frequency range is from 10^{-1} to

10^4 at the bias potential of 0.45 V. The equivalent circuit (as shown in the inset of Fig. 6) can be used to fit the spectra. R_s , C_{dl} , Z_w , R_{ct} and C_F are solution resistance, double-layer capacitance, Warburg diffusion impedance, charge-transfer resistance and Faradaic pseudo-capacitance, respectively. The impedance behavior might be dominated by three major processes occurring in the high, medium and low frequency regions, respectively [33]. At high frequency the curves are almost parallel to the real axis. It indicates that the contact resistance of the nanoparticulate film is very small. In the intermediate frequency region, the 45° line is the characteristic of ion diffusion into the porous structure of the electrode [34]. At low frequency, it is clear that the imaginary part of the impedance curves approaches a vertical line, implying an ideal capacitive behavior of the nickel oxide nanoparticulate film electrode.

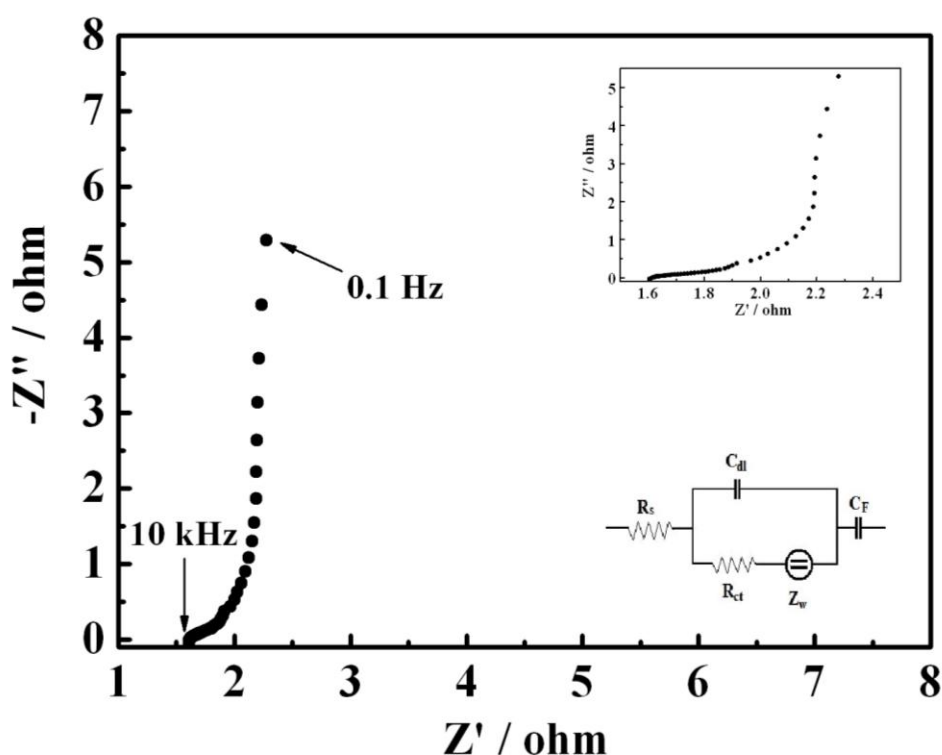


Figure 6. Nyquist plots for the nanoparticulate nickel oxide film electrode calcined at 250 °C in 1 M KOH solution. The upper right inset presents high-frequency region of the plot. The lower right inset is the equivalent circuit to fit the EIS spectra.

Besides, the specific capacitance was calculated from the low frequency data using the equation $Z'' = (2\pi fC)^{-1}$, where Z'' is the imaginary part of the impedance, f is the frequency, and C is the capacitance. The specific capacitance at 0.45 V calculated from the Z'' value at the lowest frequency ($f = 0.1$ Hz) is 1253 F g^{-1} , which is in agreement with the result of the galvanostatic discharge curves.

Long cycle life of supercapacitor is important for its practical applications. To evaluate the stability of the nanoparticulate nickel oxide film electrode calcined at 250 °C during the charge–

discharge cycle, the variety of specific capacitance with charge–discharge cycle numbers (up to 500 cycles) at a current density of 8 A g^{-1} were measured in Fig. 7. The nanoparticulate film electrode can keep 87% of maximum capacity over 500 cycles. This confirms that, within the voltage window 0.05–0.45 V, the charge and discharge processes do not seem to induce significant micro-structural changes of the film electrode as expected for pseudo-capacitance reactions.

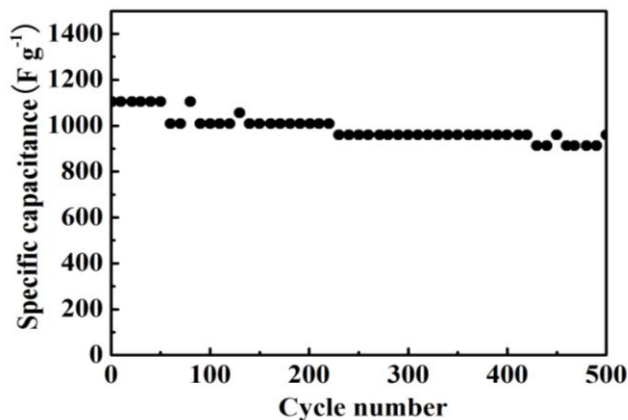


Figure 7. Cycle life data of the nanoparticulate nickel oxide film electrode calcined at $250 \text{ }^\circ\text{C}$ (8 A g^{-1})

4. CONCLUSIONS

A loosely packed nickel oxide film composed of nanoparticles was prepared by using the simple electrochemical strategy. The electrodeposited nickel hydroxide is easy to be transformed into nickel oxide at lower temperature in comparison with the one synthesized by chemical precipitation due to more intercalated water molecules or thermodynamically unstable state. Increasing calcination temperature results in the increase in grain size, thereby leads to a decrease in specific surface area and a sharp decline in the specific capacitance. The resultant nickel oxide film calcined at $250 \text{ }^\circ\text{C}$ achieves an ultrahigh specific capacitance with excellent rate capability and cycle stability. The charge-storage mechanism of the nickel oxide nanoparticulate film is not a diffusion-controlled reaction but a fast redox reaction at the electrode/electrolyte interface, suggesting their potential application as low-cost, high-performance electrode materials in supercapacitors.

ACKNOWLEDGEMENTS

The authors gratefully acknowledge the financial support offered by the National Natural Science Foundation of China (20963009 and 21163017) and Gansu Science and Technology Committee (0803RJA005).

References

1. B. E. Conway, *Electrochemical Supercapacitors, Scientific Fundamentals and Technological Application*. Plenum Press, New York (1999).

2. D. H. Jurcakova, M. Kodama, S. Shiraishi, H. Hatori, Z. H. Zhu, G. Q. Lu, *Adv. Funct. Mater.*, 19 (2009) 1800.
3. M. D. Stoller, S. J. Park, Y. W. Zhu, J. H. An, R. S. Ruoff, *Nano Lett.*, 8 (2008) 3498.
4. F. Fusalba, H.A. Ho, L. Breau, D. Belanger, *Chem. Mater.*, 12 (2000) 2581.
5. K. K. Liu, Z. L. Hu, R. Xue, J. R. Zhang, J. J. Zhu, *J. Power Sources*, 179 (2008) 858.
6. X. Dong, W. Shen, J. Gu, L. Xiong, Y. Zhu, H. Li, J. Shi, *J. Phys.Chem. B*, 110 (2006) 6015.
7. K. R. Prasad, K. Koga, N. Miura, *Chem. Mater.*, 16 (2004) 1845.
8. X. Du, C. Y. Wang, M. M. Chen, Y. Jiao, J. Wang, *J. Phys. Chem. C*, 113 (2009) 2643.
9. J. M. Luo, B. Gao, X. G. Zhang, *Materials Research Bulletin*, 43 (2008) 1119.
10. T. Y. Wei, C. H. Chen, H. C. Chien, S. Y. Lu, C. C. Hu, *Adv. Mater.*, 21 (2010) 1.
11. Z. A. Hu, Y. L. Xie, Y. X. Wang, H. Y. Wu, Y. Y. Yang, Z. Y. Zhang, *Electrochim. Acta*, 54 (2009) 2737.
12. Z. A. Hu, Y. L. Xie, Y. X. Wang, L. J. Xie, G. R. Fu, X. Q. Jin, Z. Y. Zhang, Y. Y. Yang, H. Y. Wu, *J. Phys. Chem. C*, 113 (2009) 12502.
13. W. C. Fang, *J. Phys. Chem. C*, 112 (2008) 11552.
14. C. C. Hu, W. C. Chen, K. H. Chang, *J. Electrochem. Soc.*, 151 (2004) A281.
15. D. B. Wang, C. X. Song, Z. S. Hu, X. Fu, *J. Phys. Chem. B*, 109 (2005) 1125.
16. J. W. Lang, L. B. Kong, W. J. Wu, Y. C. Luo, L. Kang, *Chem. Commun.*, 35 (2008) 4213.
17. C. C. Yu, L. X. Zhang, J. L. Shi, J. J. Zhao, J. H. Gao, D. S. Yan, *Adv. Funct. Mater.*, 18 (2008) 1544.
18. B. Gao, C. Z. Yuan, L. H. Su, S. Y. Chen, X. G. Zhang, *Electrochim. Acta*, 54 (2009) 3561.
19. M. S. Wu, M. J. Wang, J. J. Jow, *J. Power Sources*, 195 (2010) 3950.
20. M. J. Deng, F. L. Huang, I. W. Sun, W. T. Tsai, J. K. Chang, *Nanotechnology*, 20 (2009) 175602.
21. L. Cao, F. Xu, Y. Y. Liang, H. L. Li, *Adv. Mater.*, 16 (2004) 1853.
22. J. Cheng, G. P. Cao, Y. S. Yang, *J. Power Sources*, 159 (2006) 734.
23. Z. H. Liang, Y. J. Zhu, X. L. Hu, *J. Phys. Chem. B*, 108 (2004) 3488.
24. M. S. Wu, H. H. Hsieh, *Electrochim. Acta*, 53 (2008) 3427.
25. T. N. Ramesh, *J. Phys. Chem. B*, 113 (2009) 13014.
26. V. Srinivasan, J. W. Weidner, *J. Electrochem. Soc.*, 147(2000) 880.
27. G. R. Fu, Z. A. Hu, L. J. Xie, X. Q. Jin, Y. L. Xie, Y. X. Wang, Z. Y. Zhang, Y. Y. Yang, H. Y. Wu, *Int. J. Electrochem. Sci.*, 4(2009) 1052.
28. Y. G. Wang, Y. Y. Xia, *Electrochim. Acta*, 51(2006) 3223.
29. H. Kuanxin, Z.; Xiaogang, L. Juan, *Electrochim. Acta*, 51 (2006) 1289.
30. D. D. Zhao, W. J. Zhou, H. L. Li, *Chem. Mater.*, 19 (2007) 3882.
31. V. Srinivasan, J. W. Weidner, *J. Electrochem. Soc.*, 144 (1997), L210.
32. J. W. Long, K. E. Swider, C. I. Merzbacher, D. R. Rolison, *Langmuir*, 15 (1999) 780.
33. T. Y. Wei, C. H. Chen, K. H. Chang, S. Y. Lu, C. C. Hu, *Chem. Mater.*, 21(2009) 3228.
34. Z. A. Hu, Y. L. Xie, Y. X. Wang, L. P. Mo, Y. Y. Yang, Z. Y. Zhang, *Mater. Chem. Phys.* 114 (2009) 990.
35. B. E. Conway, *Electrochemical Supercapacitors, Scientific Fundamentals and Technological Application*. Plenum Press, New York (1999).